



Swelling and Fluid Transport of Re-sealed Callovo–Oxfordian Claystone

Chuanrui Wang^{1,2,3} · Jean Talandier⁴ · Frédéric Skoczylas^{1,3}

Received: 29 April 2021 / Accepted: 2 November 2021 / Published online: 8 January 2022
© The Author(s), under exclusive licence to Springer-Verlag GmbH Austria, part of Springer Nature 2021

Abstract

Several experimental methods are used to investigate the swelling capacity and transport properties of re-sealed macro-cracked Callovo–Oxfordian (COx) claystone, particularly in the absence of confining pressure. Six COx claystone samples from four different geological locations of the Bure basin (France) are tested, five of which are macro-cracked and one remains intact. Sample swelling occurs, during re-hydration with liquid water, leading to the measurement of an apparent swelling pressure. The latter is continuously recorded with a dedicated device. The asymptotic apparent swelling pressure of macro-cracked UT (transitional unit) COx is approximately 1 MPa, while it varies from 3 to 5 MPa for macro-cracked UA (clayey unit) COx. Quantitative X-ray diffraction (QXRD) analysis demonstrates that the amount of smectite, which is a swelling clay, is weakly correlated with apparent swelling pressure. Surprisingly, the interstratified illite/smectite with lower smectite content is highly correlated to apparent swelling pressure. Nitrogen isotherms data imply that the Gurvich total pore volume ($V_{Gurvich}$) and specific surface area (SSA) are highly linearly correlated with the low smectite content interstratified phase. This means that the distribution of smectite strongly affects the swelling capacity of COx. Moreover, nitrogen sorption is an easier and more effective technique than QXRD for assessing COx swelling capacity, since both $V_{Gurvich}$ and SSA have been proven as effective indicators. For both UT and UA COx, self-sealing can cause significant reductions in water permeability (K_w). In particular, UA COx shows higher sealing efficiency and faster kinetics compared to UT COx. After sealing, the equivalent crack aperture (calculated from Poiseuille's law) decreases from tens of microns to less than 1 micron. According to the gas breakthrough tests, the gas breakthrough pressure (GBP) of re-sealed macro-cracked COx is of the same order of magnitude as the equivalent capillary pressure of residual crack. This indicates that the gas migration in the re-sealed cracked COx claystone mainly occurs through the residual crack and is 'a priori' controlled by capillary processes.

Highlights

- A dedicated device was designed to study the transport and swelling properties of a sealed COx claystone under low confinement.
- The apparent swelling pressure and water permeability were continuously recorded during the sealing test due to water injection in fractures.
- Water permeability of samples decreased by orders of magnitude to almost meet the intact material permeability.
- Gas breakthrough experiments performed on sealed samples evidenced gas flow through the residual cracks.

✉ Frédéric Skoczylas
Frederic.skoczylas@centralelille.fr

¹ School of Civil Engineering and Architecture, Changzhou Institute of Technology, Changzhou, China

² University of Lille, CNRS, Centrale Lille, UCCS UMR8181, Lille, France

³ University of Lille, CNRS, Centrale Lille, LaMcube UMR9013, Lille, France

⁴ Andra, Châtenay-Malabry, France

Keywords Claystone · X-ray diffraction analysis · Swelling · Sealing · Water and gas permeability

1 Introduction

Long-lived and high-level (LL-HL) nuclear waste disposal is a worldwide technical challenge. Nowadays, the mainstream approach is to seal the nuclear waste into metal canisters then store them in underground repositories (Andra 2005; Marschall et al. 2005). The choice of geological formation is an essential issue extensively studied by industrial countries. Particularly, in France, the Callovo–Oxfordian (COx) claystone is the main candidate host rock for the geological long-term disposal of LL-HL nuclear waste, thanks to several favorable attributes such as a stable geological structure, extremely low permeability, and excellent self-sealing potential of cracks (Davy et al. 2007; Zhang et al. 2016). To solve technical challenges in the construction of underground repositories, Andra (National Agency for Nuclear Waste Management) has built a full-scale underground research laboratory (URL) at the Bure basin (cross-area of Meuse and Haute-Marne departments) in the east of France. The URL is located in the Callovo–Oxfordian formation at a depth of approx. 420–550 m. When building the nuclear waste repository structure, the host rock will be subjected to damage and desaturation due to the excavation and ventilation processes. As a consequence, a so-called Excavation Damaged Zone (EDZ) is developing around artificial structures (tunnels, galleries, etc.) and embraces numerous tensile and shear cracks with heterogeneous orientation (de La Vaissière et al. 2015). Due to the presence of cracks, the gas/water permeability of the EDZ is often several orders of magnitude higher than in undisturbed areas (Davy et al. 2007; Zhang and Rothfuchs 2004). Progressively, after the repository closure, the near-tunnel EDZ will adsorb underground water from the surrounding saturated zone. Such process can result in a decrement of water permeability and a partial restoration of safe rock properties, which is so-called self-sealing (Bernier et al. 2007). A number of researchers have been using experimental and simulation methods to study self-sealing. In laboratory experiments, mechanical effects on self-sealing are reproduced by loading macro-cracked samples with confining pressure (P_c). For instance, Davy et al. (2007) performed several P_c loading–unloading cycles on split-cracked samples and found that after one loading–unloading cycle, the crack closure became non-linear elastic and the gas permeability was largely dependent on the crack closure. Using strongly damaged samples to mimic the complex crack network of EDZ of COx claystone and Opalinus Clay, researchers found that normal stress can lead to irreversible crack closure and a gas permeability reduction up to 2 orders of magnitude (Zhang and Rothfuchs 2008; Zhang 2011). Similar stress-induced

sealing results are also observed via Micro-CT (Van Geet et al. 2008; Chen et al. 2014).

In addition to the mechanical effect, the hydration effect plays an important role in the self-sealing of EDZ. This hydration leads to the clay matrix swelling so as to induce cracks closure. In the literature, the clay matrix swelling is mainly attributed to the chemical reaction between groundwater and smectite (Mitchell and Soga 2005). Both experimental data and numerical simulations indicate that the smectite swelling can be divided into crystalline swelling and osmotic swelling. The upper capacity of crystalline swelling was equivalent to the thickness of four water molecule layers (12 Å) (Saiyouri et al. 2000; Menaceur et al. 2016), while the osmotic swelling capacity is much larger, up to approx. 100 Å (Delvaux 1992; Anderson et al. 2010; Saiyouri et al. 2004). Although results have demonstrated that smectite swelling directly contributes to the macroscopic volumetric swelling of the clayey rock, there are still some debates about this phenomenon. For instance, most of the laboratory self-sealing experiments are conducted in the presence of confining pressure. However, both external confining pressure and swelling lead to crack closure, i.e., to permeability decrease. It is, therefore, very difficult to dissociate these effects to evaluate the sole effect of swelling. Studies related to this condition are rarely found in literature. In addition, gas (mostly hydrogen) production is expected around the radioactive waste repository. This is due to the corrosion of metal facilities, water radiolysis, and other chemical reactions (Horseman et al. 1999). This leads to another important question: what is the gas migration mechanism in the re-sealed cracked COx claystone medium? The main goal of this study is to provide some answers to these questions. A dedicated experimental device has been designed to measure the apparent swelling pressure, gas and water permeability, and gas breakthrough pressure of macro-cracked COx claystone. The experimental results are analyzed in parallel with mineralogical (quantitative XRD and CEC) and nitrogen adsorption data.

2 Materials

2.1 Origin of COx Claystone Samples

Based on mineralogy proportion, the Callovo–Oxfordian formation at Meuse/Haute-Marne URL can be subdivided into three different units in order from shallow to deep: the silty-carbonated unit (USC), the transition unit (UT), and the clay unit (UA), respectively. The USC is located at the top sequence of the COx layers, around 420–445 m depth,

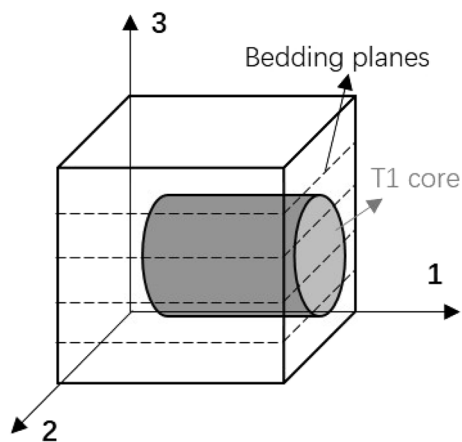


Fig. 1 Schematic diagram of transversely isotropic COx claystone



Fig. 2 Photograph of a Brazilian test (left) and the resulting diametral macro-crack (right)

and has the highest carbonates and tectosilicates contents. Beneath the USC is the UT (445–460 m), in which the proportion of each mineral can be locally highly heterogeneous. The clay-rich unit (UA) is located at the base of COx formation, at a depth of approximately 460–550 m; it covers two-thirds of the total COx formation thickness. In general, the UA has the greatest proportion of clay minerals but also contains carbonates and tectosilicates; the average contents

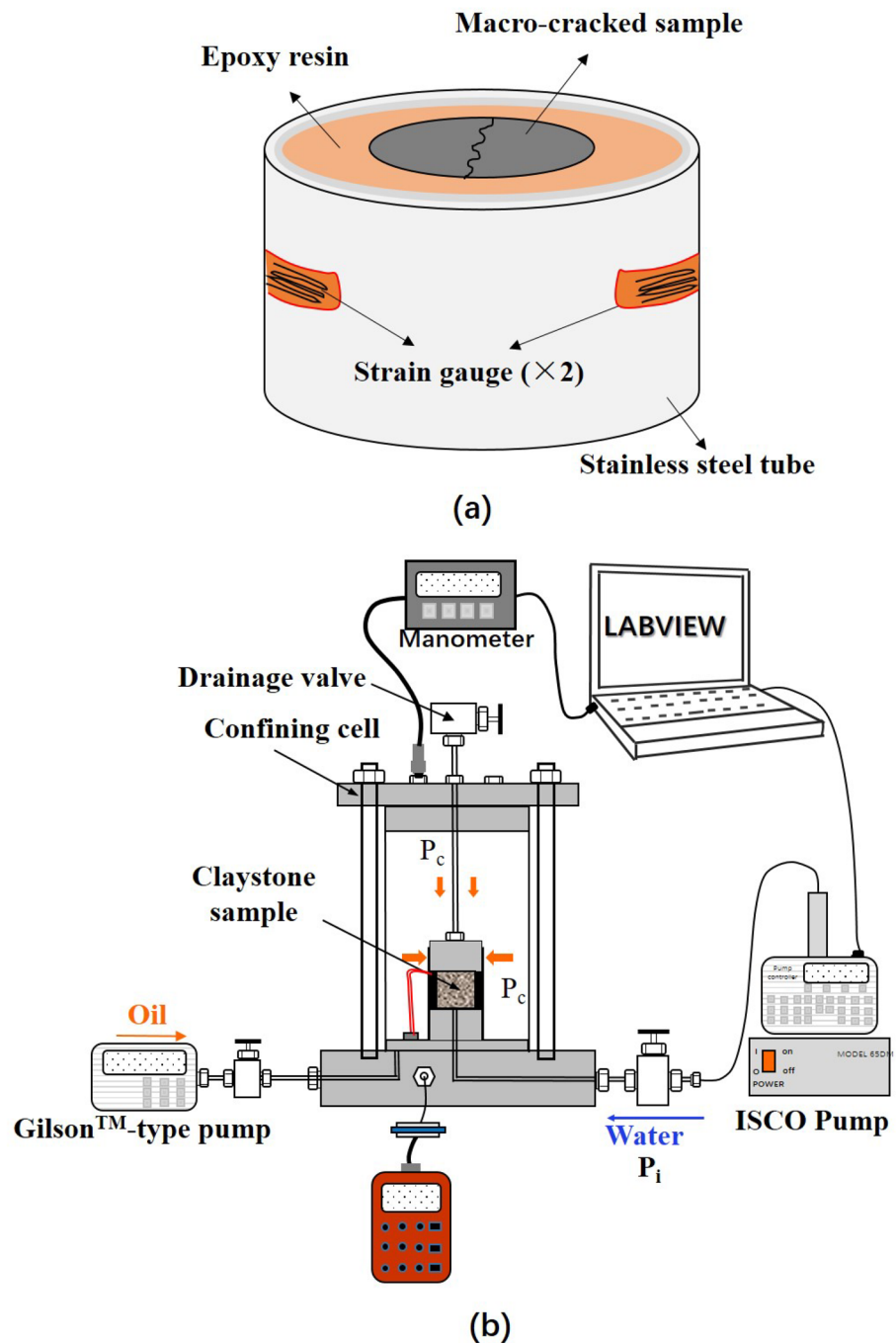
of clay minerals, carbonates and tectosilicates are around 45–50%, 27%, and 24%, respectively (Giot et al. 2019). In this research, six COx claystone samples originating from four cores were used. The four cores, provided by Andra, were extracted at different depths of the COx formation. The COx claystone is known as a transversely isotropic material, see Fig. 1 (Cariou et al. 2012). The isotropic bedding planes contain the structural axes 1 and 2, and axis 3 is perpendicular to the bedding plane. All cores were extracted along the bedding planes (i.e., axis 1) and immediately sealed in T1 cells, which were developed by Andra to allow the cores to maintain in situ saturation and a certain stress state (Conil et al., 2018). The dimensions of the original core are around 300 mm length and 75 mm diameter. From each original core, several cylindrical samples parallel to the bedding planes were retrieved to obtain representative samples that fit the experimental set-up. After coring, and before swelling and sealing test, all samples were wrapped in plastic film, sealed in vacuum bags and then immersed in oil to minimize their desaturation. The re-cored samples were of a diameter of 37 mm and a length slightly greater than 40 mm. After placing the sample in the experimental device [see Fig. 2 (a)], its length was adjusted to 40 mm by machining. The detailed preparation procedure of the sample is provided in the following subsection.

All samples were extracted from the UT and UA unit, and referenced as UT-C, UA1-C, UA2-C, UA3-C1, UA3-C2, UA3-I, where UT refers to the transition unit and UA refers to the clay-rich unit; C means that the sample is macro-cracked and I means that it is in the intact state. Table 1 summarizes the information of all tested samples, including the sample label, geological unit, damaged state, and the initial physical properties. It is worth noticing that, as the COx claystone was subjected to decompression when extracted from T1 cells and slightly de-saturated during coring, a small extent of cracks would have been generated in the samples (Duan et al. 2021). Nevertheless, these re-cored samples (without further processing or macro-cracking) are referred to “intact samples”.

Table 1 Basic information of the tested COx claystone samples

Sample label	Core number	Depth	Geological unit	Damage state	Saturation degree	Bulk density
UT-C	EST 57257	– 457 m	UT	Brazilian splitting	–	2.58 g/cm ³
UA1-C	EST 57903	– 490 m	UA	Brazilian splitting	86.8%	2.39 g/cm ³
UA2-C	EST 58128	– 490 m	UA	Brazilian splitting	85.5%	2.37 g/cm ³
UA3-C1	EST 58145	– 490 m	UA	Brazilian splitting	84.3%	2.37 g/cm ³
UA3-C2	EST 58145	– 490 m	UA	Brazilian splitting	84.3%	2.37 g/cm ³
UA3-I	EST 58145	– 490 m	UA	Intact	84.3%	2.37 g/cm ³

Fig. 3 Sketch of the experimental set-up: **a** a system consists of a steel-epoxy composite tube and a COx sample, the sample is placed in the tube center and two strain gauges are glued on the tube outer surface; **b** the hydrostatic triaxial cell used for the self-sealing experiments



2.2 Sample Preparation

2.2.1 Macro-cracking by Brazilian Splitting Test

Brazilian splitting tests were used to obtain a diametrical crack, whose aperture cannot be fully controlled. Multiple cracks were sometimes generated. After retrieving the 37 mm/40 mm samples from the original core, the Brazilian splitting tests (Davy et al. 2007) were conducted on five samples (detailed in Table 1). To avoid shattering, the side

surfaces of the sample were first wrapped with insulating tapes. The uniaxial stress was applied perpendicularly to the bedding planes to prevent cracks propagation only along the bedding surface. A typical result is shown in Fig. 3 (a). The Brazilian splitting tests were stopped when the macro-crack was created throughout the sample, see Fig. 3 (b). The numbers and diameter of cracks are significantly different from one sample to another. Apart from the split-cracked samples, an intact sample from EST 58145 was also used as the intact reference in our experiment.

2.2.2 Design of the “Stainless Steel Tube–Epoxy–Sample” System

An originally designed set-up was used to investigate the sealing efficiency of compacted bentonite/sand plugs [Liu et al. (2014)]. Innovatively, by placing the bentonite/sand plug in a stainless steel–epoxy tube, swelling occurred at almost constant volume during hydration. This allowed the asymptotic swelling pressure to be derived from the strain on the external surface of the tube. The system of “sample plug + stainless steel tube” is placed inside a triaxial cell and subjected to confining pressure. Thanks to high rigidity of the metallic tube, it is able to prevent the sample from being subjected to confining pressure. The same kind of experiment was conducted on the COx argillite since the sample was included in a rigid steel tube + epoxy resin. When water is injected, the sample swelling is partially prevented by the tube. As a consequence, the swelling sample will apply radial stress on the assemblage (tube + resin). This stress can be evaluated by calibration (see Sect. 3.3.1) and be related to a kind of swelling pressure. On the other hand, most of the swelling/sealing tests were usually performed in our laboratory with a significant confining pressure (generally from 5 to 12–14 MPa). According to Pimentel (2015), the objective of conventional swelling tests is to measure the swelling strains under constant total stress or to evaluate the intrinsic swelling pressure under constrained (zero strain) conditions. If the sealing test is conducted on a conventional experimental protocol, the results will always be directly affected by the external constraint (i.e., confining pressure) introduced. The combination of the sample swelling (due to re-hydration) and the confining pressure leads to sharp decrease in permeability. It is therefore difficult to evaluate the real role of the only swelling. In this paper, an alternative method is proposed to minimize the impact of confining pressure. As shown in Fig. 2 (a), the system consists of a stainless steel tube with an external diameter of 65 mm and a cylindrical COx claystone sample with a diameter of 37 mm, the length of the whole system is 40 mm. The claystone sample is placed in the center of the tube, and the space between tube and sample is fully filled with degassed liquid epoxy resin. The hardened resin sticks strongly to the sample surface and the tube internal surface and is considered impermeable, meanwhile it has a significant compressibility (flexibility). The internal pressure effects in the tube–epoxy structure can be evaluated with two strain gauges (with an accuracy of 10^{-6} m/m) symmetrically glued on the tube external surface, see Fig. 2 (a). Thanks to a calibration process, the strain can be converted into an “apparent swelling pressure” (P_{app}), which is an adequate indicator of the swelling process duration and amplitude. Hence, the system (tube–epoxy–cracked sample) allows to measure the swelling kinetics, and an “apparent swelling

pressure”. It can also be used to evaluate the self-sealing efficiency with water permeability measurements. On the other hand, the sample is subjected to its own swelling pressure and not to an artificial level of confining pressure. This system needs a calibration phase to obtain the relationship between gas pressure inside the tube and the strain. Both calibration and self-sealing tests are carried out with a triaxial cell, see Fig. 2 (b). The experimental procedures are detailed in Sect. 3.3.1.

3 Experimental Methodology

3.1 Mineralogical Analysis

The mineralogical analysis is carried out using two measurements: quantitative X-ray diffraction (QXRD) and Cations Exchange Capacity (CEC). Quantitative X-ray diffraction (QXRD) is used to analyze the bulk mineralogical and the subdivided clay mineral composition. For the purpose of improving the reliability of the results, two different representative parts were extracted from each sample, then analyzed and averaged. The detailed representative sample preparation and measurement procedures are illustrated in Appendix (Sect. 6.1).

Cation exchange capacity (CEC) is an inherent characteristic of a clayey material (such as soil and claystone), which refers to the ability of the solid to hold exchangeable cations in a saline aqueous solution. This property is mainly impacted by the content of clay minerals and organic matter (Mitchell and Soga 2005). Empirically, the CEC value of 2:1 type clay minerals (e.g., smectite) is approx. 80–120 meq/100 g, which is higher than 1:1 type clay minerals (e.g., kaolinite), around 1–10 meq/100 g. The CEC varies from 100 to 300 meq/100 g for the organic matter (Al-Ani and Sarapää 2008). To determine the most active

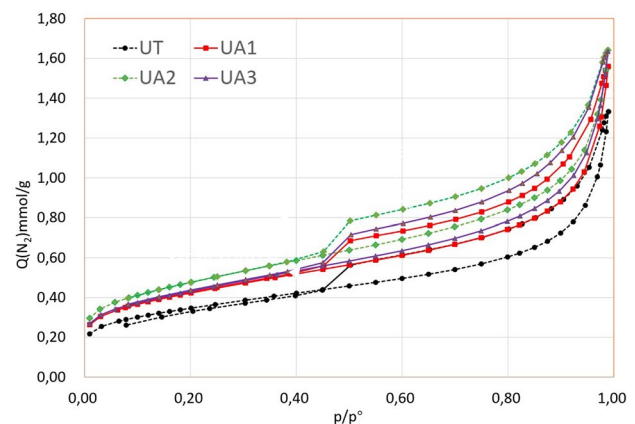


Fig. 4 Nitrogen adsorption results of tested samples

mineral component of the CO_x claystone during hydration, CEC analysis was simultaneously performed for each sample subjected to QXRD. The experimental techniques are exposed in Appendix (Sect. 6.2).

3.2 Nitrogen Physisorption Measurement

Nitrogen adsorption/desorption experiments are used to obtain pore information of the tested CO_x samples. The main goal is to acquire the nitrogen isotherms, by recording the adsorbed nitrogen quantity at different relative nitrogen pressures. These isotherms are summarized in Fig. 4, the sample preparation and measure procedures are illustrated in Appendix 6.3. These isotherms data can be used and analyzed with different theories to derive a series of textural parameters such as the total pore volume ($V_{Gurvich}$) and the Specific Surface Area (SSA), which were selected for this study. $V_{Gurvich}$ is the pore volume that is determined under the validity of Gurvich rule (Ongari et al. (2017)): when the relative pressure $p/p_0 \geq 0.995$, the adsorbed nitrogen has a molar density of the liquid state at the operational temperature, and has no interaction with the solid framework. The $V_{Gurvich}$ is computed by:

$$V_{Gurvich} = \frac{n_{N_2}^{ads}}{\rho_{N_2}^{liq}}, \quad (1)$$

where $n_{N_2}^{ads}$ is the adsorbed amount of nitrogen (g of nitrogen/g of CO_x), $\rho_{N_2}^{liq}$ is the liquid nitrogen density, 0.808 g/cm³. Theoretically, $V_{Gurvich}$ is an underestimated value of the total connected pore volume as nitrogen cannot fill the micro-pores with a diameter smaller than the N₂ molecules.

Specific Surface Area (SSA) is derived by the Brunauer–Emmett–Teller (BET) theory, which is an optimization of Langmuir theory. The BET theory can give the monolayer adsorbed capacity (Q_m) and the adsorbent's specific surface area (SSA). Data from the straight part of isotherms to fit the empirical BET equation are used for these calculations (Seemann et al. 2017). One should notice that the BET theory is an approach based on several assumptions; thus, the derived Q_m and SSA cannot be treated as the real physical properties (Lahn et al. 2020; Seemann et al. 2017). However, with well-controlled experimental conditions, they are still useful and effective for characterizing pore structure and to compare different materials (Rouquerol et al. 2007; Thommes and Katiea 2014).

3.3 Self-Sealing Experiments

Four results were recorded during the self-sealing measurements: evolution of the “apparent swelling pressure” (P_{app}), initial gas permeability (K_{inigas}), change of water permeability (K_w), and gas breakthrough pressure (GBP) after self-sealing. All the experiments were carried out in a temperature-controlled room to minimize the effect of temperature, with an average value of 21°C. To better simulate the interaction between the clay mineral and the underground water, a specially made synthetic water was used in all self-sealing tests. The detailed mineralogical composition is shown in Table 2.

The self-sealing experiment was carried out with a modified triaxial cell. The system (tube–epoxy–cracked sample) is first wrapped with a rubber jacket then installed in the triaxial cell [Fig. 3 (b)]. For saturation purpose, a Gilsons™ pump is used to control the confining pressure (P_c) of 4 MPa, the sample is then subjected to a wetting environment. More precisely, the saturation process is achieved by injecting synthetic water into the cylindrical sample from one end surface until it passes through the sample. The drainage valve [Fig. 3 (b)] is then closed to obtain uniform water pressure through the whole sample. This pressure (P_i) is of 0.5 MPa, which is lower than the confining pressure to avoid any leakage around the tube.

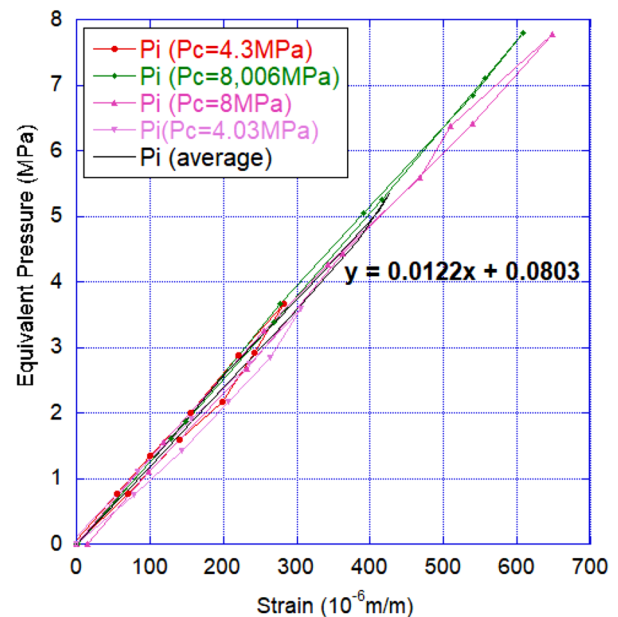


Fig. 5 An example of tube calibration

Table 2 Mineral composition of the synthetic water (provided by Andra)

Mineral	NaCl	NaHCO ₃	KCl	CaSO ₄	MgSO ₄	Na ₂ SO ₄	CaCl ₂	Total
Concentration (g/L)	1.95	0.13	0.035	0.63	1.02	0.08	0.7	4.545

The drainage valve is periodically opened to measure the sample water permeability (see Sect. 3.3.3).

3.3.1 Apparent Swelling Pressure Measurement

The tube was calibrated before conducting the self-sealing experiment. This is done with gas pressure inside the tube (*P_{internal}*) linked to the corresponding average strain of both gauges $\epsilon_{average} = (\epsilon_1 + \epsilon_2)/2$. A linear relationship between *P_{internal}* and strain is shown in Fig. 5. To improve the accuracy, several internal pressure loading/unloading cycles were performed on each tube submitted to various confining pressure. A special test was performed for which the gas pressure was applied on the “epoxy resin + stainless steel tube”. The strains obtained were close to those recorded when the gas pressure was directly applied in the steel tube. Thanks to the tube calibration, the direct measurement data (strains of the two gauges) are constantly converted into *P_{app}*. *P_{app}* is recorded until its stabilization.

Water can easily flow through the sample at the beginning of the test due to the presence of macro-cracks. Closing the drainage valve allows the sample to swell under (quasi) uniform water pressure without any perturbative drying risk. For the sample sizes used, the swelling process usually lasts for two weeks–one month. It should be underlined that *P_{app}* is the total stress applied on the tube so it also depends on pore pressure (*P_{pore}*). This pressure was of the same value (0.5 MPa) for all tests. *P_{app}* can then be decomposed as follows:

$$P_{app} = P_{pore} + P_{swell} - \Pi_{epoxy}, \quad (2)$$

where Π_{epoxy} represents the effect of epoxy resin on the transmission of sample swelling pressure to the tube. This value has been revealed to be very low during the calibration test. In any case, the presence of resin does not affect the comparison of *P_{app}* between different samples. As a consequence, the measured *P_{app}* is not the genuine value induced from sample swelling but it is still a reliable result for assessing and comparing the COx claystone swelling behavior (and kinetics).

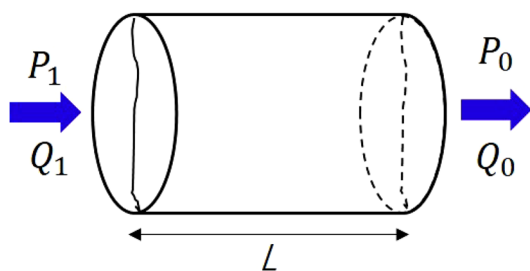


Fig. 6 Schematic diagram of permeability test

3.3.2 Permeability Assessment Techniques

Some transfer properties of the cracked samples were measured: the initial gas permeability (*K_{inigas}*) and the water permeability (*K_w*) over time. The initial gas permeability is measured with argon gas under steady flow rate. The injection pressure is *P₁* (at upstream side) since the sample is freely drained at *P₀* = *P_{atm}* at the downstream side (see Fig. 6). A Bronkhorst gas flowmeter with an accuracy of 0.01 ml/min is connected to the downstream side for the permeability test. Once a stabilized gas flow is detected, the classic Darcy’s law for gas phase is applied to calculate the *K_{inigas}*:

$$K_{inigas} = \frac{2\mu QL P_0}{A(P_1^2 - P_0^2)}, \quad (3)$$

where μ is the dynamic viscosity of argon at 21 °C, equals to 2.2×10^{-5} Pa s, *Q* is the volume flow rate measured at the downstream sample side, *L* is the sample length, *A* is the cross-sectional area of sample, *P₁* is the upstream gas pressure, and *P₀* is the downstream atmospheric pressure.

The self-sealing efficiency was accessed via two properties: water permeability and gas breakthrough pressure (GBP). They were selected because they can quite easily be captured for the experimental procedure. Water permeability was periodically measured to be compared to the “intact” one. The latter is often in the range [10^{-19} m², 5×10^{-21} m²], for laboratory measurements (M’Jahad et al. 2017). Therefore, for assessing the swelling-induced permeability decrease, the change of water permeability (*K_w*) is recorded over time as the sample hydrates and swells. If the differential pressure between the sample inlet and outlet (ΔP) is known, the water permeability can be calculated using Darcy’s law for liquid phase by recording the water flow rate *Q*, the equation is as follows:

$$K_{water} = \frac{\mu QL}{A \Delta P}. \quad (4)$$

Equation 4 is valid under permanent flow rate, which is assumed to be really obtained at the end of the sealing (stable strain values) during several days. Before this stabilization it is observed a sharp and rapid drop of the water flow rate *Q*. This flow rate was then converted into water permeability *K_w* to facilitate the result reading and to illustrate the sealing effects. It is worth underlining that the *K_w* value measured before stabilization is not the intrinsic water permeability as the effects of transient flow are not taken into account. This is therefore an apparent or approximate value of the water permeability *K_w* obtained every one–two days, until the end of swelling. The drainage valve remained open during each permeability evaluation and was closed again as soon as the measurement was completed.

3.3.3 Gas Breakthrough Measurement Techniques

GBP was chosen as being another swelling indicator. The gas breakthrough tests were carried out immediately after the swelling stabilized. The measured GBP data were compared to values obtained on different samples during previous laboratory experiments (M'Jahad et al. 2017). In terms of methodology, two methods are presented in the literature to study the gas migration in (partially) saturated porous materials: the steady-state approach and the non-steady-state approach (Horseman et al. 1999; Amann-Hildebrand et al. 2016; Liu et al. 2014). The non-steady-state approach leads to shorter test durations and can provide both breakthrough and residual pressures; however, it was chosen to use the steady-state approach in the GBP tests (i.e., slow increase of gas pressure until gas is detected at the downstream sample side). It is often assumed that this technique leads to more accurate GBP value and in the present case, it was thought to better reproduce the in situ case for which gas pressure is supposed to increase slowly. When both P_{app} and K_w were stabilized, the ISCO water pump was dismantled and replaced by an argon injection system. To start the GBP test, argon is injected from the upstream side of the saturated sample, with 0.2 MPa increment every 24 h. The downstream (i.e., the drainage valve of the cell in Fig. 3) is initially closed, which results in downstream pressure increase. This increase may be due to expelled water from the sample (i.e., “pushed” by the upstream gas pressure) and/or to the gas (argon) breakthrough. A gas detection device was then used to detect (or not) this breakthrough. Detection is performed by placing an argon detector (accurate to $\pm 0.1 \mu\text{l/s}$) close to the drainage valve. This valve is opened and the detector gives an indication whether argon is present at

the downstream side. The valve is closed again after this operation. Different physical processes can be successively observed: water expulsion due to gas intrusion, discontinuous (transient) gas flow, and continuous gas flow (Liu et al. 2014). The inlet gas pressure leading to continuous gas flow is defined as being the breakthrough gas pressure of the tested sample.

4 Results and Discussion

4.1 Mineralogical Characterization

The bulk mineralogical compositions and the subdivided 2:1 clay minerals are summarized in Table 3. Through the QXRD analysis, the bulk mineralogical composition results demonstrate that the COx claystone contains similar primary minerals for both UA and UT types. They are mainly silicates (like quartz), carbonates (like calcite), and 2:1 clay minerals (layered clay content). The secondary mineral phases (such as kaolinite, chlorite, K-feldspar, pyrite, etc.) are also present in the COx claystone with lower quantities. Results show that the total clay content is slightly lower for the UT core (with values ranging between 30.4% and 39.3%) than for the UA cores (values in the range 40.1–50.0%). Moreover, they also demonstrate that, among all clay minerals, the illite/smectite mixed layers R1 and R0 constitute the vast majority. Indeed, the illite/smectite mixed layers are divided into two types: the R1-I/S, with 70% illite and 30% smectite, and the R0-I/S, with a proportion of 22% illite and 78% smectite. In R1-I/S, smectite is arranged in regular alternance with illite. Among these, smectite is the only one reputed to be a swelling clay.

Table 3 Quantitative XRD and CEC analysis for different cores of the tested COx claystone (in mass percentage)

Sample	EST 57257-1	EST 57257-2	EST 57903-1	EST 57903-2	EST 58128-1	EST 58128-2	EST 58145-1	EST58145-2
Geological unit	UT	UT	UA	UA	UA	UA	UA	UA
Carbonates	33.4	26.6	29.5	27.7	22.1	21.0	22.6	22.7
Tectosilicates	33.7	32.2	28.6	26.8	26.9	26.9	29	28.6
Secondary minerals	2.6	1.9	1.9	1.8	2.1	1.9	1.7	1.9
Kaolinite	/	/	2.2	2.7	3.3	3.4	2.9	3.0
Chlorite	0.9	1.2	1.1	1.4	1.5	1.7	1.7	1.7
2:1 clay minerals	29.5	38.1	36.8	39.6	44.1	44.9	42.2	42.0
of which illite and muscovite	2.5	9.0	4.7	12.9	13.1	14.3	18.8	20.2
of which R1 illite/smectite (70/30)	14.2	13.3	23.5	20.6	22.6	23.2	24.2	23.4
of which R0 illite/smectite (22/78)	12.9	15.8	8.5	6.1	8.5	7.4	6.2	6.0
Total smectite	14.3	16.3	13.7	10.9	13.4	12.7	12.1	11.7
Total clay minerals	30.4	39.3	40.1	43.7	49.0	50.0	46.8	46.7
CEC (meq/100 g)	16.8	19.2	14.6	13.1	17.6	16.8	15.2	14.2

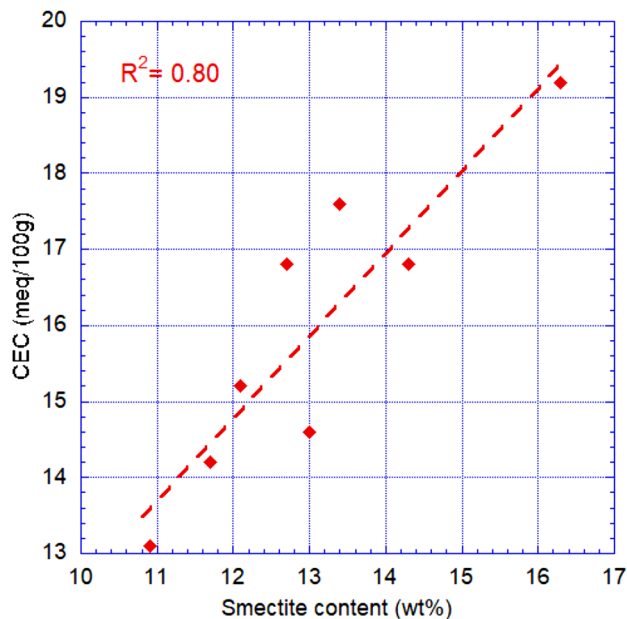


Fig. 7 Relation between the CEC value and the smectite content

In the 2:1 clay minerals group, the subdivided mineral contents are not consistent with the trend of the overall 2:1 clay minerals content. In other words, the subdivided mineral contents in 2:1 clay minerals are contrasted and there is no dominant mineral. In the presence of aqueous solution, specific minerals among the 2:1 clay minerals will be substituted with exchangeable cations in aqueous solution, and the interlayer spacing of which expands as a result of the adsorption of water molecules which are carried by the exchangeable cations. Therefore, to determine the most chemically active (i.e., the most swelling-related) mineral, the Cations Exchange Capacity (CEC) was carried out. Results demonstrate that the total smectite contents are linearly related to the CEC value, with a Pearson correlation coefficient (R^2) of 0.8035, see Fig. 7. Hence, in COx claystone, smectite can be considered as the most swelling-related mineral among all 2:1 clay minerals. For the whole set of UA samples, the difference in the content of smectite was not significant and results in similar CEC values. The smectite content of the two UT representative samples (EST57257-1 and EST57257-2) is slightly higher than for UA samples. But this cannot be generalized as the mineral composition of UT COx claystone varies greatly from one location to another [Andra (2005)].

4.2 Apparent Swelling Pressure (P_{app})

After a long period of geological evolution, the COx claystone matrix has been highly compacted and its hydration swelling is essentially due to the increase of pore volume. It was observed that crystalline swelling and osmotic swelling

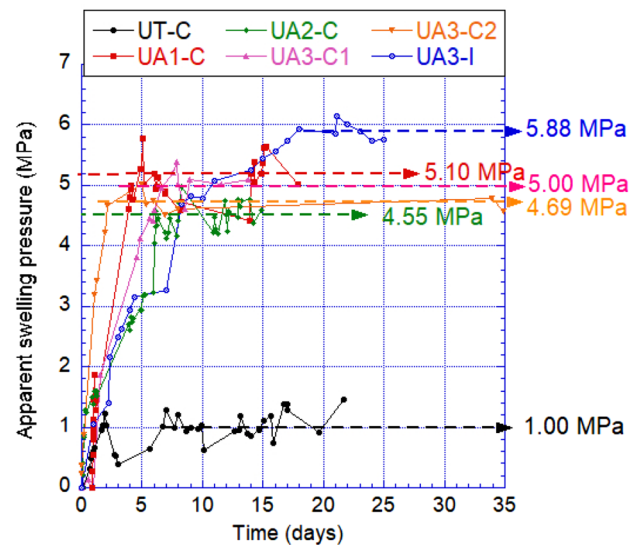


Fig. 8 Evolution of apparent swelling pressure of the tested COx claystone sample

occur in the infra-clay micro-pores and inter-clay particle meso-pores, respectively (Saiyouri et al. 2000; Menaceur et al. 2016). In this study, the measured apparent swelling pressure (P_{app}) is the consequence of swelling coupled with a limited volume expansion of the COx sample. The P_{app} change with time was recorded for each test and given in Fig. 8. For the macro-cracked samples, the difference between P_{app} value of UA and UT samples is quite significant: the P_{app} of the UT-C is around 0.99 MPa, while for the four tested UA samples (UA1-C, UA2-C, UA3-C1, and UA3-C2), the value of P_{app} is in the range of 4.55–5.10 MPa. For comparison purposes, the swelling pressure of intact sample UA3-I was also measured (5.88 MPa) in parallel with the macro-cracked samples. From the viewpoint of kinetics, the swelling time of UA3-C1 and UA3-C2 are both around five days, while it is 17 days for the intact sample UA3-I. Such difference in kinetics indicates that the presence of macro-cracks creates more water–mineral contact area inside the sample, which accelerates the swelling process. P_{app} of UA3-I, 5.88 MPa, is relatively higher than P_{app} for UA3-C1 and UA3-C2. The difference in P_{app} between macro-cracked and intact samples is around 15%. One plausible interpretation of such difference is that the crack network leads to more swelling space, i.e., there is a logical decrease in P_{app} . On a global point of view, P_{app} is lower than the expected (but not measured) value of the “real” swelling pressure, which was theoretically estimated to be 12–14 MPa (Zhang et al. 2020). One has nevertheless to mention that this estimation was obtained for undisturbed (i.e., in situ) material under zero volumetric strain condition. Obviously, these conditions do not apply in the present case as samples used are partially uncompacted and the experimental device

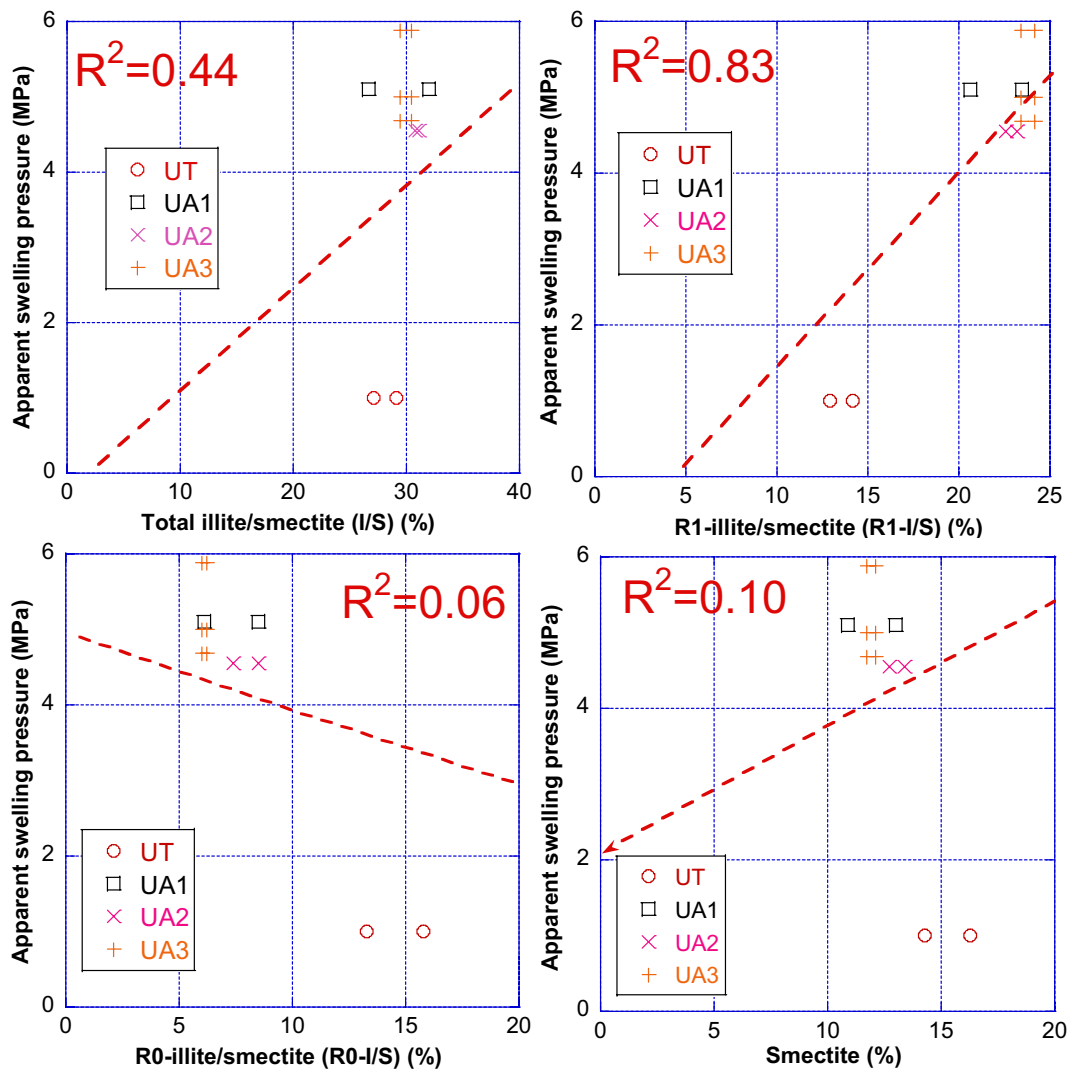


Fig. 9 Apparent swelling pressure vs. specific clay mineral content

does not allow the zero volumetric strain condition. It is why the term “ P_{app} ” was chosen. Despite being lower than the ‘real’ swelling pressure, it allows useful comparisons between different samples and conditions.

Knowing the quantitative XRD results, it can be analyzed whether there is a specific mineral that affects the swelling capacity of the COx claystone. To this purpose, the mass content of each clay mineral is linearly related (in the least squares sense) to the apparent swelling pressure P_{app} , see Fig. 9. The total interstratified I/S exhibits an ambiguous relationship with P_{app} , with an Pearson coefficient R^2 of 44%. It is observed that the clay mineral most related to the swelling pressure P_{app} is R1-I/S, with an R^2 of 83%. On the opposite, the Pearson coefficient between smectite content and P_{app} is of only 10%. The lowest correlation ($R^2=6\%$) is obtained for R0-I/S, although it contains 78% smectite in mass. These results demonstrate that the total

smectite amount and the content in mixed I/S clay are not the driving factors of the magnitude of P_{app} at the laboratory scale. Compared to other clay minerals in COx claystone, the R1-I/S structure that makes it easier for water molecules to enter the clay layers seems to be a more significant factor.

To verify this argument, nitrogen adsorption tests were carried out and two important properties were obtained, namely the Gurvich pore volume ($V_{Gurvich}$) and the specific surface area (SSA). $V_{Gurvich}$ and SSA reflect the ability of water molecules to come into contact with minerals (particularly with smectite). The $V_{Gurvich}$ pore volume corresponds to the total amount of water molecules that can fill the inter-layer pores. The specific surface area SSA represents the surface area of water molecules that can be adsorbed on clay minerals. The nitrogen adsorption results ($V_{Gurvich}$ and SSA) are linearly correlated with the apparent swelling pressure P_{app} (Fig. 10). P_{app} is linearly correlated with $V_{Gurvich}$ and

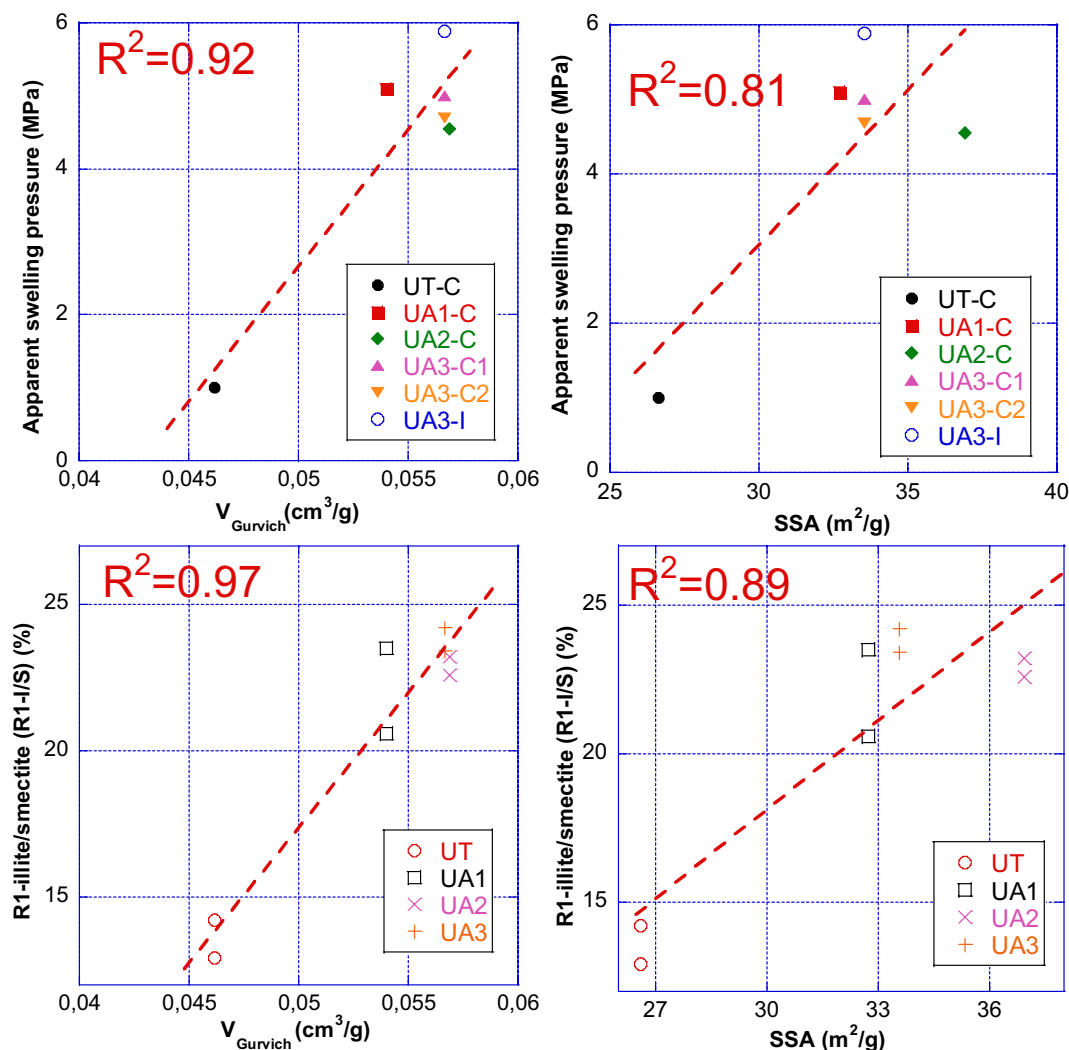


Fig. 10 Correlation of nitrogen adsorption data with apparent swelling pressure: **a** P_{app} vs. $V_{Gurvich}$ **b** P_{app} vs. SSA **(a)** R1-I/S vs. $V_{Gurvich}$ **(b)** R1-I/S vs. SSA

SSA, with R^2 of 92% and 81% respectively, see Fig. 10 (a) and (b). If we relate the R1-I/S content (which revealed to be the most strongly correlated with P_{app}) with $V_{Gurvich}$ and SSA, a remarkably linear relationship was found with both nitrogen sorption properties ($R^2 = 97\%$ and 87% , respectively), see Fig. 10 (c) and (d). As smectite is not present as a single phase in the COx claystone (Andra 2005), a plausible explanation is that the smectite present in R1-I/S is more favorable for water–smectite contact, because it contributes to a greater pore volume and a larger specific surface area. Therefore, it can be supposed that the spatial arrangement of smectite seems to be more important than its content. Hence, using CEC values to assess the swelling capacity is inaccurate, as regards the macroscopic swelling of COx claystone.

Moreover, a nitrogen sorption test is easier to be carried out than QXRD. It would be interesting to confirm that

for clay rocks, both $V_{Gurvich}$ and SSA are highly correlated with the clay material swelling capacity.

4.3 Permeability Assessment

Gas and water permeability (evolution) were used for two different purposes. Coupling gas permeability (K_g) with Poiseuille law is able to evaluate a “mean” crack initial width. Water permeability was mainly recorded to be compared to the water permeability of “intact” COx argillite. If, after swelling, both values (i.e., macro-cracked sample and intact material) are close to each other, it would evidence an efficient self-sealing. Moreover, if water flow through the crack is assumed after swelling, the

Table 4 Initial gas permeability and water permeability of the tested sample

	UT-C	UA1-C	UA2-C	UA3-C1	UA3-C2	UA3-I
Initial K_g (m^2)	3.85×10^{-13}	1.79×10^{-13}	6.04×10^{-14}	1.08×10^{-13}	–	1.37×10^{-17}
Initial aperture (calculated with initial K_g) (μm)	32.89	26.57	20.71	24.48	–	–
Initial K_w (m^2)	1.7×10^{-14}	2.88×10^{-14}	1.44×10^{-14}	1.18×10^{-14}	8.31	2.48×10^{-20}
Initial aperture (calculated with initial K_w) (μm)	18.11	21.58	17.14	16.02	14.26	–
Final K_w (m^2)	2.7×10^{-17}	7.44×10^{-20}	4.67×10^{-20}	3.72×10^{-20}	1.24×10^{-20}	1.24×10^{-20}
Final aperture (calculated with final K_w) (μm)	2.11	0.296	0.253	0.235	0.163	–

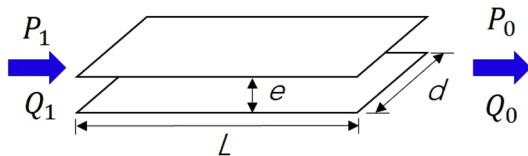


Fig. 11 Simplified cracks consist of two parallel planes with a distance of e

permeability can also lead to a “final” crack width. This is developed in the following.

4.3.1 Gas Permeability

The initial value of K_g was measured under almost no lateral pressure, thanks to the presence of stainless steel tube. As a consequence, K_g comes from a gas flow that is supposed to mainly take place through the macro-crack. This assumption is logical as the obtained results gave gas permeability 3–4 orders of magnitude higher than the intact one, see Table 4 (also see Duan et al. 2021). As the lateral stress applied on the cracked sample is very low, the gas permeability occurs in an opened crack and can be analyzed to evaluate its initial width. The initial K_g of macro-cracked samples (Table 4) are between $10^{-13} m^2$ and $10^{-15} m^2$. It is noteworthy that the K_g of UA3-2 is not reported due to experimental measurement problem. For the intact sample UA3-I, the initial K_g is of $1.37 \times 10^{-17} m^2$ that is consistent with previous tests (Zhang and Rothfuchs (2004)).

4.3.2 Use of Poiseuille Law

Poiseuille’s law was used to obtain what can be called the “crack equivalent aperture (e)”. To this purpose, the crack is simply modeled as two parallel planes and e is the distance between both (Fig. 11). It is obviously far from reality as the crack surface roughness plays a major role in its permeability (Chen et al. 2021), but remains a useful assumption to compare samples and to follow crack aperture evolution.

[Fig. 11. about here.]

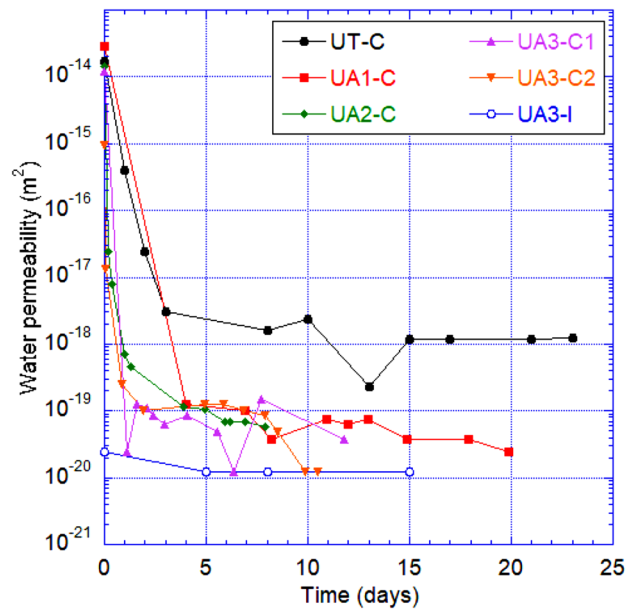


Fig. 12 Variation of water permeability with time

Poiseuille’s law leads to the fracture calculation of the fluid flow rate Q_1 and Q_0 . For an incompressible liquid in steady flow rate:

$$Q = Q_1 = Q_0 = \frac{dx e^3}{12 \mu L} (P_1 - P_0) . \tag{5}$$

And for a compressible perfect gas:

$$Q_0 = \frac{P_1}{P_0} Q_1 = \frac{dx e^3}{12 \mu L} \times \frac{(P_1^2 - P_0^2)}{2 P_0} . \tag{6}$$

With Eqs. 4 and 3 and when the material matrix permeability is low (compared to the crack aperture “permeability”), it comes for both gas and liquid:

$$KA = \frac{dx e^3}{12} \tag{7}$$

or

$$e = \sqrt[3]{3 K \pi d} . \tag{8}$$

Table 5 Summary of equivalent capillary and gas breakthrough pressure

Sample label	Sealed equivalent aperture (μm)	Equivalent capillary pressure (MPa)	GBP (MPa)
UT-C	2.11	0.06	0–0.2
UA1-C	0.296	0.49	0.8–0.89
UA2-C	0.253	0.58	1.3–1.46
UA3-C1	0.235	0.62	1.00–1.23
UA3-C2	0.163	0.893	1.0–1.2
UA3-I	–	–	6.2–6.4

4.3.3 Water Permeability

Gas permeability was a unique measure used to quantify the equivalent initial gas aperture. Water permeability was recorded in parallel with P_{app} to identify the end of the swelling process. The latter is assumed as soon as both K_w and P_{app} are stable. Evolution of K_w can be found in Fig. 12 and compared with Fig. 8. On a global point of view, there was a strong and rapid swelling for UA-C type samples, and this is consistent with a sharp drop in permeability during around the first 5 days. Both phenomena then stabilized slowly for 20–25 days. This observed parallelism is logical as swelling leads to crack closure. At the end of the process, water permeability of UA-C samples has decreased by 5–6 orders of magnitude. It is still slightly higher than initial values reported for intact sample but all in the range [10^{-19} m^2 , 10^{-20} m^2]. This evidences the swelling efficiency on self-sealing. The UT-C sample exhibited a low swelling pressure (1 MPa) and its final water permeability stabilized at 10^{-18} m^2 . This value is one order of magnitude higher than the one measured on intact UT sample. For this sample, it can be concluded that the self-sealing is partial as despite a strong decrease in its water permeability the latter remains significantly higher than the intact one.

Initial values of water permeability (at the beginning of water injection) are given in Table 4. They are all almost one order of magnitude less than the initial gas permeability. As a result, the initial crack aperture derived from K_w is smaller than what was calculated with K_g . Contrary to gas, water is chemically active with clay (also the case with concrete) and K_w smaller than K_g is usual with COx claystone. On the other hand, swelling is likely to occur very quickly therefore having an immediate impact on permeability. As aforementioned, the final values at the end of the swelling reveal an efficient self-sealing of the UA samples as they are now close to the intact material on a permeability point of view.

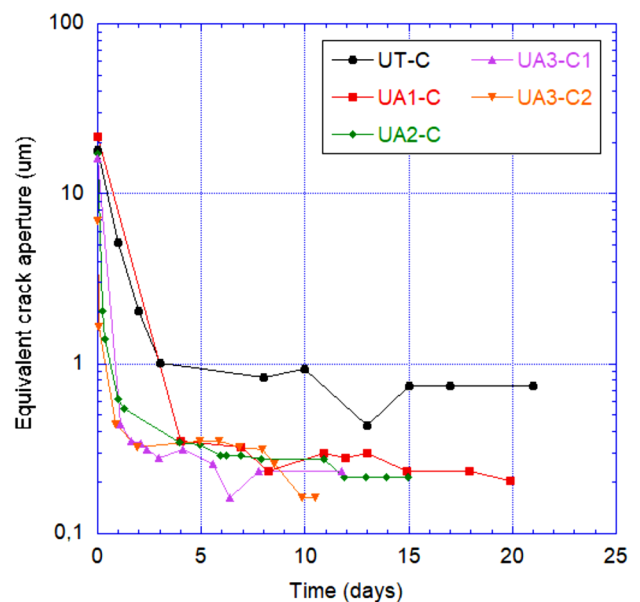
4.4 Gas Breakthrough Pressure (GBP)

4.4.1 Laboratory Results

When P_{app} and K_w were both stabilized, it was considered that the sample had reached full saturation and the gas breakthrough test was immediately performed. The GBP value of each test is shown in Table 5. After sealing, the GBP results for the saturated COx demonstrate distinctive features. The first one is that for macro-cracked samples, a significant difference in GBP values between UA and UT is observed. The GBP of UT COx is around 0–0.2 MPa, while the value of UA COx range from 0.8 to 1.46 MPa. This confirms that UA COx possesses a better sealing efficiency than UT COx claystone, which is consistent with the observation of the initial K_w and equivalent crack aperture. The other investigation is that by comparing UA3-C1, UA3-C1 and UA3-I, it is found that the GBP of intact sample is 4–6 times higher than those of sealed macro-cracked samples. This demonstrates for the UA COx that even if the induced self-sealing brings the sample back to a very low K_w (close to the intact one), the gas transfer properties do not meet those in the undisturbed state. As a result, coupled with P_{app} and K_w , GBP reveals to be a strong complementary tool to evaluate the sealing efficiency.

4.4.2 Equivalent Capillary Pressure

The displacement of a gas phase in a saturated porous media is a complex process. Four gas migration mechanisms have been proposed by (Marschall et al. 2005), including

**Fig. 13** Equivalent single crack aperture evolution of all tested samples

diffusion, visco-capillary flow, pore dilatancy flow, and gas fracturing. A series of experiments carried out in our laboratory (such as M'Jahad et al. 2017) had led us to think that capillary phenomena (i.e., a part of the porous network is emptied from its saturating water by gas pressure) are preponderant for saturated COx claystone. Based on previous studies, it is reasonable to assume that the gas migration mechanism in the re-sealed macro-cracked COx would be capillary gas transport through the sealed crack. To evaluate whether this assumption is plausible, calculation of the equivalent crack aperture e_{gw} were performed with the final K_w (Fig. 13 and Table 5). One can find that e_{gw} (both UA and UT COx) decreased from tens of microns to below one micron after sealing. Thus, it can be supposed that, during a GBP experiment, gas would use the easier path to cross the sample, i.e., the sealed crack. Assuming again that this crack is composed of two parallel planes with a width equal to e_{gw} , Laplace's law is used to calculate the capillary pressure P_{cap} :

$$P_{cap} = \frac{2\gamma_{gw}}{e_{gw}} \times \cos \alpha, \quad (9)$$

where γ_{gw} is the gas–water interfacial tension, 72.9×10^{-3} N/m at 20 °C; α is the gas/water contact angle, here it is taken at 0. P_{cap} is assumed to be the necessary gas pressure to push water away from the crack. It can then be compared with GBP (Table 5). Even if lower than the real measured value, it can be underlined that P_{cap} remains in the same order of magnitude than GBP. Given the simplicity (two parallel planes) of the crack geometry and the fact that the whole sample water permeability is due to water flow in the crack, these results can be regarded as quite convincing. On the other hand, they confirm the hypothesis of GBP due to capillary phenomena. The GBP value of intact sample UA3-I was also measured, which was between 6.2 and 6.4 MPa. A rough calculation with GBP value equal to P_{cap} , compared with Laplace's law, leads to a mean pore radius of the intact sample around 0.023 μm (23 nm). This result is consistent with what can be found in the literature (Song et al. 2015, 2016).

5 Conclusions

This contribution investigates the self-sealing behavior of macro-cracked COx claystone, using quantitative X-ray diffraction (QXRD), nitrogen adsorption measurements, and a series of originally designed swelling and sealing experiments. Both UT and UA COx claystone are used for QXRD and nitrogen adsorption tests: QXRD results give us a comprehensive understanding of the bulk mineral and subdivided clay mineralogical composition of different cores; nitrogen adsorption isotherms data imply the information

of pore volume ($V_{Gurvich}$) and specific surface area (SSA) of samples with different mineralogy composition. Using a specially designed experimental system, the swelling and sealing experiments of macro-cracked and intact samples are carried out in the absence of external confining pressure. Through this experiment, the change of apparent swelling pressure and permeability during re-saturation and the gas breakthrough pressure (GBP) after sealing have been measured. These direct measurement data would provide important references for numerical reproduction. Combining all the results from different experiments, several interesting results can be underlined as follows:

- (1) During re-saturation, the apparent swelling pressure (P_{app}) of both macro-cracked and intact samples logically increased with time. By comparing macro-cracked samples from different geological positions, the P_{app} of UT COx is approximately 1 MPa, while it varies from 3 to 5 MPa for UA COx. By comparing samples from the same core, macro-cracked samples exhibit faster kinetics than the intact sample, while intact sample exhibits a slightly higher P_{app} than macro-cracked samples. Such difference is mainly attributed to the presence of cracks that increases the water–clay mineral contact area and generates more space for swelling.
- (2) Relating P_{app} to specific clay mineral content, the smectite (swelling mineral) content does not seem to be the main influential factor, while the content of R1-I/S exhibits good linearity with P_{app} . Nitrogen adsorption data demonstrate that both $V_{Gurvich}$ and SSA are well linearly related to P_{app} and R1-I/S content, which implies that the effective water–mineral contact space and specific surface area are the key factors for COx swelling, and not simply the content of smectite fraction. That is to say, estimating the swelling capacity of COx by CEC values will lead to inaccurate results. From a viewpoint of testing technology, the $V_{Gurvich}$ and SSA that derived from nitrogen adsorption data have been proven to be simple and effective parameters for assessing COx swelling capacity. This should be verified and completed with other experiments.
- (3) For both UT and UA COx, the presence of macro-cracks results in a significant increment of permeability, up to 2–4 orders of magnitude for K_g and 5–6 orders of magnitude for K_w . Self-sealing of macro-cracked COx can cause significant reductions in water permeability (K_w) synchronously with the increase in P_{app} . The final water permeability of UA samples is reduced by five orders of magnitude and close to that of the intact sample, while the final K_w of UT sample is reduced by four orders of magnitude and stabilized at around one–two orders of magnitude higher than the one measured (or reported) for intact sample. Such results demonstrate

that even in the absence of high level of confinement, the clay mineral swelling can still lead to the macro-cracked COx claystone reseal to some degree. Besides, UA COx shows faster kinetics compared to UT COx, which can be attributed to the impact of R1-I/S content.

- (4) After sealing, the results of gas breakthrough tests illustrate that the GBP of UT COx is around 0–0.2 MPa, while the value of UA COx range from 0.8 to 1.46 MPa. This confirms that UA COx possesses a better sealing efficiency than UT COx even for gas transport, which is consistent with the observation of K_w decrease. Compared with P_{app} and K_w , GBP is more sensitive to the sample integrity. Using Poiseuille Law, the GBP value of the sealed sample is in the same order of magnitude as the equivalent capillary pressure of residual cracks, which indicates that the gas migration in the sealed COx claystone would mainly occur through the residual sealed crack and is controlled by capillary phenomena.

Appendix

Quantitative X-ray Diffraction (QXRD)

To determine the bulk mineralogical composition, first, the representative sample of claystone are crushed manually into powders, combined with internal standard (0.2 g/g Al_2O_3 serving as the accuracy control). The powders are subsequently micronized, milled in ethanol and spray dried. After that, the powders are loaded in a sample holder by side loading and measured by X-ray diffraction (in this study, a $CuK\alpha$ radiation was used). The subsequent weight quantification of each mineral can be performed based on the Rietveld method (Zhou et al. 2018). For the detailed 2:1 clay minerals analysis, a chemical treatment was first used to remove cementing agents of powders, the powder size is selectively separated to below 2 μm by means of centrifugation. Each type of powders will be saturated with Ca^{2+} . Thus, all expandable clay mineral cations are exchanged to Ca^{2+} and this greatly facilitates identification and quantification of the different clay mineral species. The oriented preparations are made by sedimentation on a porous ceramic plate. The preparations yield highly oriented clay particles. They are subsequently analyzed by X-ray diffraction for the measurement of the first reflections (001) of the clay minerals.

Generally, the accuracy of non-clay mineral composition can be controlled within 1%, while it is difficult to assess the accuracy of clay mineral composition due to the lack of standard materials. The bias of XRD results is mainly associated with the mistaken of quantifying illite as smectite (Seemann et al. 2017).

Cation Exchange Capacity

The representative part of samples (around 5 g) is retrieved from different cores, and first dried at 110 °C and then weigh noted. All samples were subsequently stirred and dispersed in ultrapure water with Co (III)-hexamine, following the method described in (Meier and Kahr 1999). The exchange progress was accomplished by means of placing the sample and solution in an overhead shaker until the exchange reaction was completed. All samples were then homogenized after ultrasonic treatment and the absorption of the supernatant liquid was measured using a spectrophotometer. The cation exchange capacity of each sample was derived by the difference of concentration between the solution and supernatant liquid. For each sample, the procedure was repeated several times to increase the accuracy of the results. The detailed methodology was elaborated interpreted in the literature, for instance, (Meier and Kahr 1999). The value of CEC is quantified in milligram equivalents (meq) of exchangeable cations per 100 g of the dry sample or in millimoles of exchangeable cations per grams (mmol/g) of dry sample (Song et al. 2017).

Nitrogen Physisorption

For each measurement, the representative COx sample (2–4 g) is first manually crushed and sieved to obtain fragments of 63–400 μm size. All the treated sample fragments are degassed for 12 h, then heated in a vacuum environment at 130 °C for at least 12 h. The adsorption/desorption measurement is carried out on a Micromeritics ASAP2020 machine. Using nitrogen at a constant temperature of 77 K, 31 relative pressure points during adsorption and 24 relative pressure points during desorption are recorded, within a relative pressure interval of 0.001–0.995 p/p^0 . The equilibration is regarded as the pressure change over 10 s is less than 0.01% of the average pressure during the latter interval. And the saturation pressures (i.e., p^0) are re-calibrated independently for each step.

Acknowledgements The authors are grateful to Andra (French Agency for Nuclear Waste Management) for providing samples and funding this research program. We also acknowledge the Qmineral Company for its assistance in Quantitative XRD and CEC analysis.

Declarations

Conflict of interest The authors declare that there is no conflict of interest linked to this study.

References

- Al-Ani T, Sarapää O (2008) Clay and clay mineralogy. Geological survey of Finland
- Amann-Hildebrand A, Dietrichs JP, Krooss BM (2016) Effective gas permeability of Tight Gas Sandstones as a function of capillary pressure—a non-steady-state approach. *Geofluids* 16:367–383
- Anderson RL, Ratcliffe I, Greenwell HC et al (2010) Clay swelling—a challenge in the oilfield. *Earth Sci Rev* 98:201–216
- ANDRA (2005) Dossier 2005 Argile. ANDRA, Collection les Rapports. <https://www.andra.fr/sites/default/files/2018-02/265.pdf>
- Bernier F, Li XL, Bastiaens W et al (2007) SELFRAC: Fractures and Self-healing within the excavation disturbed zone in clays. In: Final Technical Publishable Report EUR 22585, European Commission
- Cariou S, Duan Z, Davy CA et al (2012) Poromechanics of partially saturated COx argillite. *Appl Clay Sci* 56:36–47
- Chen GJ, Maes T, Vandervoort F et al (2014) Thermal Impact on damaged boom clay and opalinus clay: permeameter and isostatic tests with μ CT scanning. *Rock Mech Rock Eng* 47:87–99
- Chen W, Han Y, Agostini F et al (2021) Permeability of a macro-cracked concrete effect of confining pressure and modelling. *Materials* 14:862. <https://doi.org/10.3390/ma14040862>
- Conil N, Talandier J, Djizanne H et al (2018) How rock samples can be representative of in situ condition: a case study of Callovo-Oxfordian claystones. *J Rock Mech Geotech Eng* 10:613–623
- Davy CA, Skoczylas F, Barnichon JD, Lebon P (2007) Permeability of macro-cracked argillite under confinement: gas and water testing. *Phys Chem Earth Parts a/b/c* 32:667–680
- de La Vaissière R, Armand G, Talandier J (2015) Gas and water flow in an excavation-induced fracture network around an underground drift: a case study for a radioactive waste repository in clay rock. *J Hydrol* 521:141–156
- Delvaux B (1992) Morphology, texture, and microstructure of halloysitic soil clays as related to weathering and exchangeable cation. *Clays Clay Miner* 40:446–456. <https://doi.org/10.1346/CCMN.1992.0400409>
- Duan Z, Skoczylas F, Wang C, Talandier J (2021) Hydric cycle impacts on COx argillite permeability and young's modulus. *Rock Mech Rock Eng* 54:1129–1147. <https://doi.org/10.1007/s00603-020-02258-1>
- Giot R, Auvray C, Talandier J (2019) Self-sealing of claystone under X-ray nanotomography. *Geol Soc London Spec Publ* 482:213–223
- Horseman ST, Harrington JF, Sellin P (1999) Gas migration in clay barriers. *Eng Geol* 54:139–149
- Lahn L, Bertier P, Seemann T, Stanjek H (2020) Distribution of sorbed water in the pore network of mudstones assessed from physisorption measurements. *Microporous Mesoporous Mater*. <https://doi.org/10.1016/j.micromeso.2019.109902>
- Liu J-F, Davy CA, Talandier J, Skoczylas F (2014) Effect of gas pressure on the sealing efficiency of compacted bentonite–sand plugs. *J Contam Hydrol* 170:10–27
- M'Jahad S, Davy CA, Skoczylas F, Talandier J (2017) Characterization of transport and water retention properties of damaged callovo-oxfordian claystone. *Geol Soc London Spec Publ* 443:159–177
- Marschall P, Horseman S, Gimmi T (2005) Characterisation of gas transport properties of the opalinus clay, a potential host rock formation for radioactive waste disposal. *Oil Gas Sci Technol Rev IFP* 60:121–139
- Meier LP, Kahr G (1999) Determination of the cation exchange capacity (CEC) of clay minerals using the complexes of copper(II) Ion with triethylenetetramine and tetraethylenepentamine. *Clays Clay Miner* 47:386–388
- Menaceur H, Delage P, Tang AM, Talandier J (2016) The status of water in swelling shales: an insight from the water retention properties of the callovo-oxfordian claystone. *Rock Mech Rock Eng* 49:4571–4586
- Mitchell JK, Soga K (2005) Fundamentals of soil behavior, 3rd edn. Wiley, New Jersey
- Ongari D, Boyd PG, Barthel S et al (2017) Accurate characterization of the pore volume in microporous crystalline materials. *Langmuir* 33:14529–14538
- Pimentel E (2015) Existing methods for swelling tests—a critical review. *Energy Procedia* 76:96–105
- Rouquerol J, Llewellyn P, Rouquerol F (2007) Is the bet equation applicable to microporous adsorbents? *Studies in surface science and catalysis*. Elsevier, pp 49–56
- Saiyouri N, Hicher P-Y, Tessier D (2000) Microstructural approach and transfer water modelling in highly compacted unsaturated swelling clays. *Mech Cohes Frict Mater* 5:41–60
- Saiyouri N, Tessier D, Hicher P-Y (2004) Experimental study of swelling in unsaturated compacted clays. *Clay Miner* 39:469–479
- Seemann T, Bertier P, Krooss BM, Stanjek H (2017) Water vapour sorption on mudrocks. *Geol Soc London Spec Publ* 454:201–233
- Song Y, Davy CA, Troadec D et al (2015) Multi-scale pore structure of COx claystone: towards the prediction of fluid transport. *Mar Pet Geol* 65:63–82
- Song Y, Davy CA, Bertier P, Troadec D (2016) Understanding fluid transport through claystones from their 3D nanoscopic pore network. *Microporous Mesoporous Mater* 228:64–85
- Song Y, Davy CA, Bertier P et al (2017) On the porosity of COx claystone by gas injection. *Microporous Mesoporous Mater* 239:272–286
- Thommes M, Katie A C (2014) Physical adsorption characterization of nanoporous materials: progress and challenges. *Adsorption* 20:233–250
- Van Geet M, Bastiaens W, Ortiz L (2008) Self-sealing capacity of argillaceous rocks: review of laboratory results obtained from the SELFRAC project. *Phys Chem Earth Parts a/b/c* 33:S396–S406
- Zhang C-L (2011) Experimental evidence for self-sealing of fractures in claystone. *Phys Chem Earth Parts a/b/c* 36:1972–1980
- Zhang C-L, Rothfuchs T (2004) Experimental study of the hydro-mechanical behaviour of the callovo-oxfordian argillite. *Appl Clay Sci* 26:325–336
- Zhang C-L, Rothfuchs T (2008) Damage and sealing of clay rocks detected by measurements of gas permeability. *Phys Chem Earth Parts a/b/c* 33:S363–S373
- Zhang Y, Lebedev M, Sarmadivaleh M et al (2016) Swelling effect on coal micro structure and associated permeability reduction. *Fuel* 182:568–576
- Zhang F, Cui YJ, Conil N, Talandier J (2020) Assessment of swelling pressure determination methods with intact callovo-oxfordian claystone. *Rock Mech*. <https://doi.org/10.1007/s00603-019-02016-y>
- Zhou X, Liu D, Bu H et al (2018) XRD-based quantitative analysis of clay minerals using reference intensity ratios, mineral intensity factors, rietveld, and full pattern summation methods: a critical review. *Solid Earth Sci* 3:16–29

Publisher's Note Springer Nature remains neutral with regard to jurisdictional claims in published maps and institutional affiliations.